Girolline is a sequence context-selective modulator of eIF5A activity

Tilman Schneider-Poetsch, Yongjun Dang, Wakana Iwasaki, Mayumi Arata, Yuichi Shichino, Ali Al Mourabit, Celine Moriou, Daniel Romo, Jun O Liu, Takuhiro Ito, et al.

nature communications

Article

https://doi.org/10.1038/s41467-024-54838-2

Girolline is a sequence context-selective modulator of eIF5A activity

Received: 22 June 2023

Accepted: 21 November 2024

Published online: 10 January 2025

Check for updates

Tilman Schneider-Poetsch[1] ✉, Yongjun Dang[2], Wakana Iwasaki[3], Mayumi Arata[4], Yuichi Shichino[5], Ali Al Mourabit[6], Celine Moriou[6], Daniel Romo[7], Jun O. Liu[8], Takuhiro Ito[3], Shintaro Iwasaki[5,9] & Minoru Yoshida[1,4,10,11] ✉

Natural products have a long history of providing probes into protein biosynthesis, with many of these compounds serving as therapeutics. The marine natural product girolline has been described as an inhibitor of protein synthesis. Its precise mechanism of action, however, has remained unknown. The data we present here suggests that girolline is a sequence-selective modulator of translation factor eIF5A. Girolline interferes with ribosome-eIF5A interaction and induces ribosome stalling where translational progress is impeded, including on AAA-encoded lysine. Our data furthermore indicate that eIF5A plays a physiological role in ribosome-associated quality control and in maintaining the efficiency of translational progress. Girolline helped to deepen our understanding of the interplay between protein production and quality control in a physiological setting and offers a potent chemical tool to selectively modulate gene expression.

Natural products have proven valuable tools in the elucidation of ribosome-catalyzed protein biosynthesis. Translation inhibitors have become potent therapeutics for the treatment of bacterial infections. The current pandemic highlights the need for specific medications in the fight against infectious diseases. This need is not limited to the treatment of viral or bacterial infections but extends to parasitic maladies.

Girolline[1] (Giro, also known as girodazole, Fig. 1a) was first isolated from the New Caledonian marine sponge *Cymbastela cantharella (originally called Pseudaxinyssa cantharella Lévi)* and described as an anti-tumor agent as well as having activity against malaria[2–6]. X-Ray analysis of the camphorsulfonate salt of natural Giro established its absolute configuration as (*2S,3S*). A search for minor metabolites from the same sponge made it possible to obtain additional quantities of Giro for biological and mode of action studies[7,8].

Giro was characterized as a translation inhibitor several decades ago, with some suggestion of it inhibiting the termination process[5,9]. Although its binding site on the large ribosomal subunit had been identified[10], neither mechanism of action nor therapeutic use have ever been thoroughly explored.

Recent developments in methodology have enabled a deeper understanding of the mode of action of translation modulators not only in terms of their molecular mechanism but also in their cellular context, providing a comprehensive overview of changes to the entire

[1]Chemical Genomics Research Group, RIKEN Center for Sustainable Resource Science, Wako, Saitama, Japan. [2]Basic Medicine Research and Innovation Center for Novel Target and Therapeutic Intervention, Ministry of Education, The Second Affiliated Hospital of Chongqing Medical University, College of Pharmacy, Chongqing Medical University, Chongqing, China. [3]Laboratory for Translation Structural Biology, RIKEN Center for Biosystems Dynamics Research, Yokohama, Kanagawa, Japan. [4]Drug Discovery Seed Compounds Exploratory Unit, RIKEN Center for Sustainable Resource Science, Wako, Saitama, Japan. [5]RNA Systems Biochemistry Laboratory, RIKEN Cluster for Pioneering Research, Wako, Saitama, Japan. [6]Institut de Chimie des Substances Naturelles, CNRS UPR 2301, Univ. Paris-Sud, Université Paris-Saclay, Gif-sur-Yvette, France. [7]Department of Chemistry and Biochemistry, Baylor University, One Bear Place, Waco, USA. [8]Department of Pharmacology and Molecular Sciences, The Johns Hopkins University School of Medicine, Baltimore, MD, USA. [9]Department of Computational Biology and Medical Sciences, Graduate School of Frontier Sciences, The University of Tokyo, Kashiwa, Chiba, Japan. [10]Office of University Professors, The University of Tokyo, Bunkyo-ku, Tokyo, Japan. [11]Collaborative Research Institute for Innovative Microbiology, The University of Tokyo, Bunkyo-ku, Tokyo, Japan. ✉e-mail: tsp@riken.jp; yoshidam@riken.jp

https://doi.org/10.1038/s41467-024-54838-2

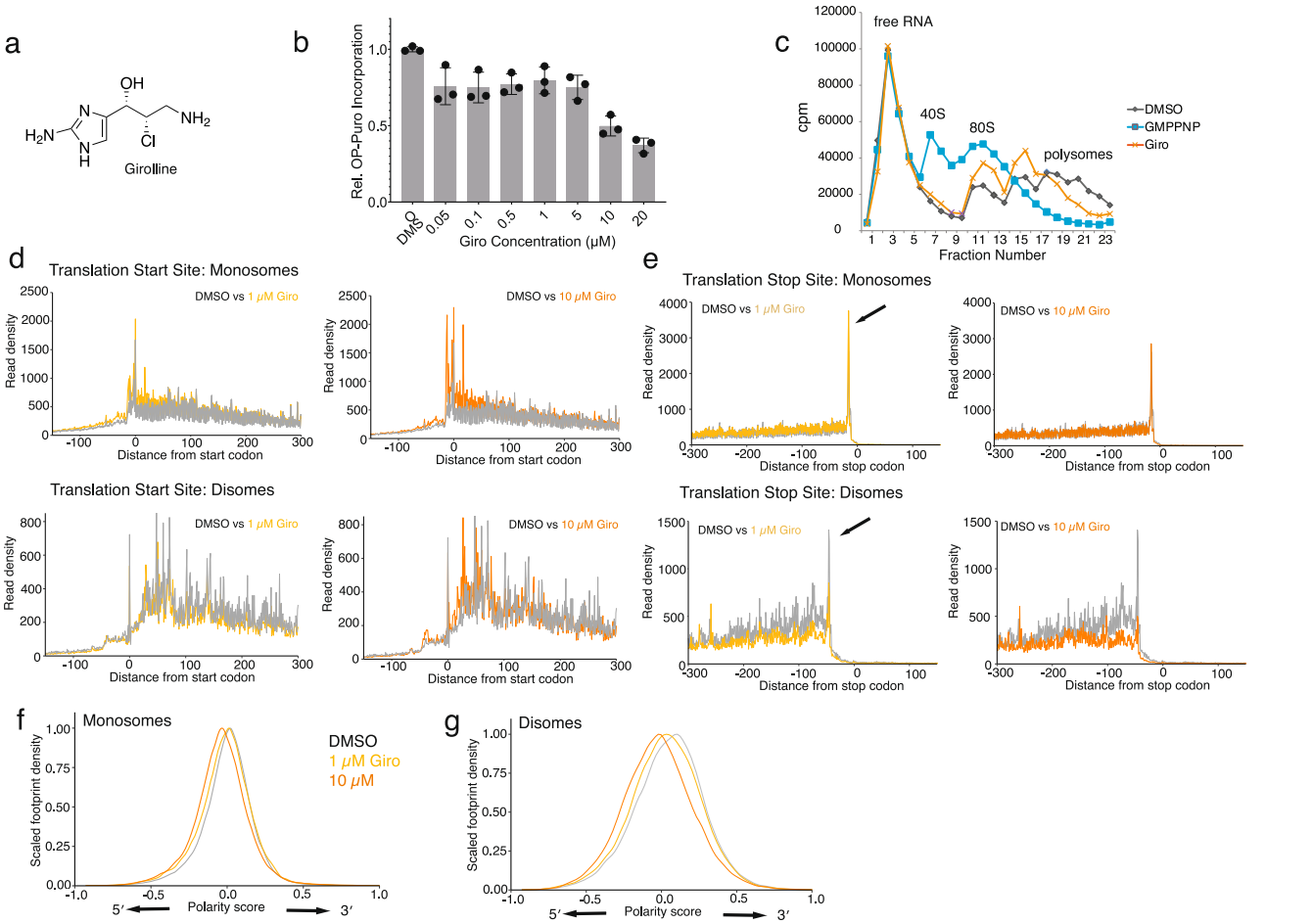

Fig. 1 | Giro stalls elongating ribosomes. a Molecular Structure of Giro **b** Measurement of translation by metabolic labeling with O-propargyl puromycin (OP-puro) in the presence of increasing doses of Giro. The experiment was conducted in triplicate with background deduction. Error bars denote the standard deviation of the mean. The data shown is representative of three independently conducted experiments. **c** In vitro polysome profiling of [^{32}P]-labeled globin mRNA in rabbit reticulocyte lysate in the presence of DMSO (gray), the non-hydrolyzable GTP analog GMP-PNP (blue) or Giro (orange). Reactions were ultracentrifuged through a sucrose gradient and fractionated. The RNA content of each fraction was measured by scintillation counting. Ribosomal populations are marked in the graph. Data is representative of three independently conducted experiments. **d** Metagene analysis of averaged ribosome profiling reads around the translation start site for both monosomes and disomes. Overlay of 1 μM (yellow) or 10 μM (orange) Giro-treated samples with DMSO control (gray). Reads were normalized by total read count and their 5′ ends were mapped from −150 to 300 nucleotides from the start codon. **e** Metagene analysis of average ribosome profiling reads mapped from − 300 to 300 nucleotides from the translation stop site. Since the ribosomal A-site is displaced by ~ 15 nucleotides (monosomes) or ~ 45 nucleotides (disomes) from the 5′ end of the read, the peaks appear shifted from the stop codon (indicated by arrows on graphs for 1 μM Giro treatment). **f** Monosome polarity shift analysis in the presence of 1 μM and 10 μM Giro. The distribution of ribosome density was evaluated from 5′ to 3′ for all open reading frames. A negative polarity score indicates a higher ribosome density towards the translation start site. **g** Polarity shift analysis for disome data. Source data are provided within the Source Data file.

proteome and translatome[11–13]. Previous mechanistic studies on translation modulators were often hampered by describing the molecule's activity solely in an isolated in vitro system, which precluded observing the compound's physiological effect. In particular, sequence-specific modulation of translation often went undetected. Ribosome profiling[12,14] overcomes this issue and has brought to light the context-dependent effects of translation inhibitors[13]. Context-dependent inhibition of translation provides an avenue to selectively target part of the proteome rather than inhibiting translation in a global manner.

Employing ribosome profiling and recently developed disome profiling[15–18], we revisited Giro to explore its activity across the translatome. In this study, we could confirm that Giro interferes with protein synthesis but did not find evidence for inhibition of translation termination[3]. Rather, Giro acts in a sequence-dependent context and causes increased ribosomal stalling on amino acid sequences where translation appears to slow down. It interferes with the ability of translation elongation factor eIF5A to interact with the ribosome.

eIF5A represents one of the most puzzling proteins regulating the synthesis of polypeptides. Originally identified as an initiation factor, it appears to play a far more important role in translation elongation[19–25]. So far, it is also the only protein known to carry a hypusine post-translational modification, derived from spermidine and attached to a Lys residue (K50 in humans) in a two-step process by the dedicated enzymes dehydroxyhypusine synthetase (DHS) and dehydroxyhypusine hydroxylase (DOHH)[21,26–28]. While eIF5A is not essential for translation in vitro, eIF5A constitutes an essential gene, and loss of either eIF5A or DHS is lethal[19,29]. Defects in eIF5A or its hypusination are associated with various disease states, including neurodegeneration and cancer[30–33]. In particular, the decrease of hypusination in the aging process has been associated with mitochondrial degeneration[34,35]. eIF5A appears to aid the ribosome through structurally challenging amino acid stretches, such as poly-Pro sequences[23,36]. Yet, the role of hypusine remains incompletely understood, and specific chemical probes into eIF5A function are lacking, while indirect probes targeting the polyamine or hypusination machinery leave a lot to be desired[37].

https://doi.org/10.1038/s41467-024-54838-2

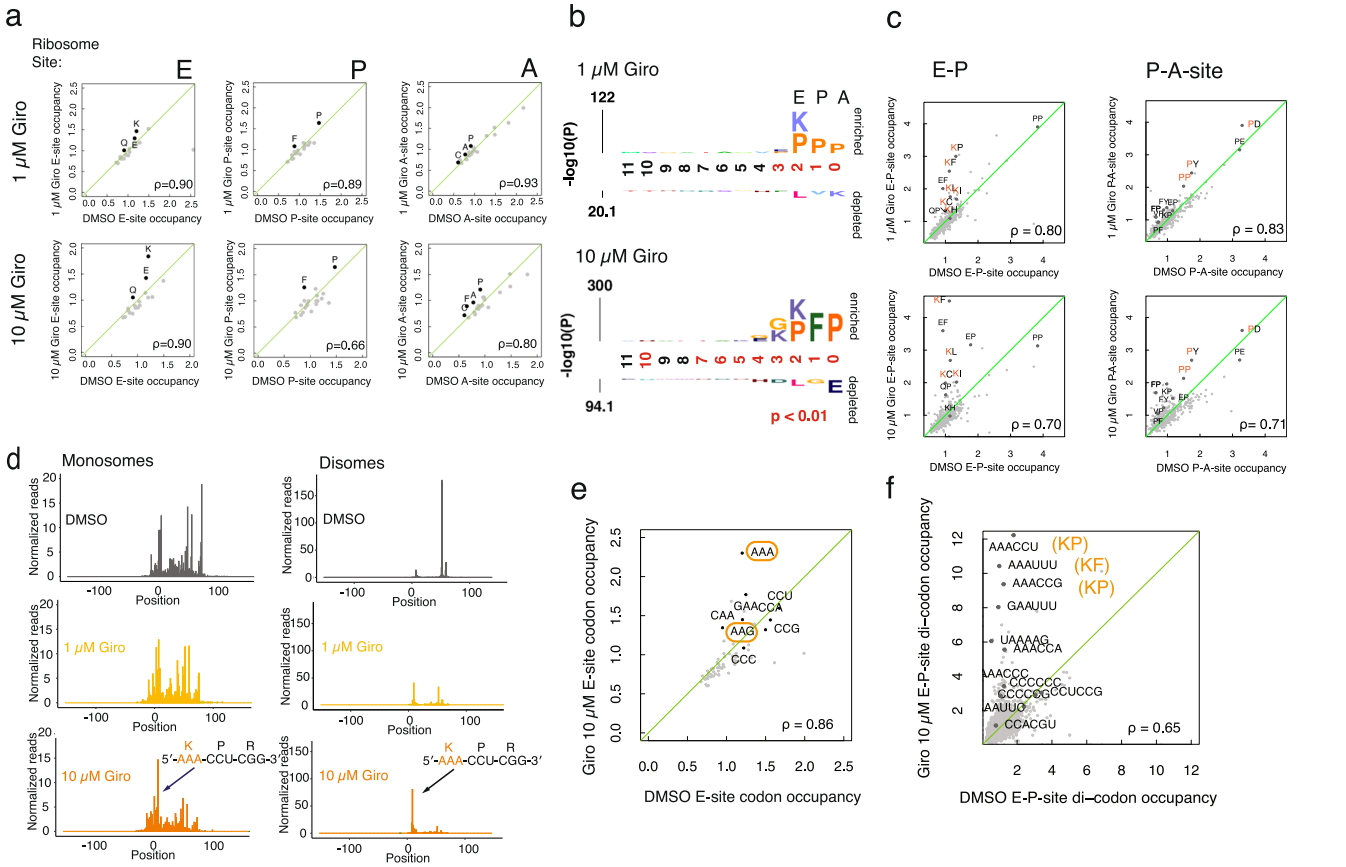

Fig. 2 | Sequence-selective stalling. a Evaluation of increased E, P, or A-site occupancy of disome fractions treated with 1 μM or 10 μM Giro. Occupancy scores for each amino acid in the presence of Giro (*y*-axis) were plotted against DMSO control (x-axis). Points above the green line indicate overrepresented amino acids in the presence of Giro. **b** Amino acid enrichment analysis using the k-mer probability logo (kpLogo) web tool, which also considers positional interdependencies. Letters above the line indicate the most significantly enriched amino acids in each position. Red numbers indicate a calculated *p*-value below 0.01 using a one-sided two-sample Student *t* test. **c** Further enrichment analysis, focusing on dipeptides occupying E and P-site or P and A-site together. Dipeptide combinations above the green line are overrepresented. Enriched Lys in the E-site or enriched Pro in the A and P-sites are highlighted in orange. **d** Monosome and Disome footprints mapped across the COX6C ORF for DMSO control (gray), 1 μM Giro (yellow), and 10 μM Giro (orange). The main stall site under Giro treatment is marked with an arrow in the map for 10 μM Giro treatment with the nucleotide and amino acid sequence in E, P, and A-site indicated. **e** Codon-wise enrichment analysis of disome data for the ribosomal E-site in 10 μM Giro treated cells. The two Lys codons AAA and AAG are outlined in orange. AAG accounts for about 58% of lysines in the human genome, AAA for ~ 42%. **f** Di-codon enrichment analysis for E and P-site. Enriched dipeptides Lys-Pro (from codons AAA-CCU and AAA-CCG) and Lys-Phe (AAA-UUU) were entered in orange. Source data are provided within the Source Data file.

The function of eIF5A largely mirrors that of bacterial translation factor EF-P[38,39]. Both proteins bind between the ribosomal P and E-sites, while their post-translational modifications hypusine (eIF5A) or R-β-lysinyl-hydroxylysine (EF-P) extend toward the peptidyl transfer center, pushing the CCA-end of the P-site peptidyl-tRNA into a more productive conformation, thereby entropically increasing the rate of amino acid incorporation[40–42]. While EF-P extends toward the small ribosomal subunit's E-site, eIF5A's interaction is limited to the large subunit. In addition, EF-P is mainly specific to $tRNA^{Pro}$ and $tRNA^{fMet}$, while eIF5A acts on a wider range of tRNAs.

Our data suggest a role of eIF5A in connecting ribosomal progress with quality surveillance. It appears eIF5A aids translational progression and prevents ribosomes from stalling, thereby blocking premature activation of the ribosome-associated quality control pathway (RQC). Giro modulates eIF5A behavior, causing increased ribosomal stalling on, but not limited to, Pro containing stretches and AAA-encoded Lys codons, especially when preceded by basic amino acid stretches.

Results

Ribosome stalling induced by Giro

First, we set out to characterize Giro's inhibitory activity on protein synthesis in mammalian cells. Through metabolic labeling of newly synthesized proteins with *O*-propargyl-puromycin (OP-puro) (Fig. 1b), an aminoacyl-tRNA mimic carrying a click-chemistry compatible alkyne which allows conjugation to a fluorescent dye, we did observe a decrease in protein synthesis by Giro in a dose-dependent manner. However, we also noticed that Giro did not inhibit translation to the same extent as conventional translation elongation inhibitors such as cycloheximide (CHX) or anisomycin (ANS) (Supplementary Fig. 2a, b). When looking at the in vitro distribution of ribosomal populations via sucrose density gradient centrifugation of [^{32}P]-labeled rabbit β-globin mRNA in rabbit reticulocyte lysate (Fig. 1c), we observed an increase in the early polysome fraction. This increase in polysomes contradicted general translation initiation inhibition, which often results in polysome depletion. For comparison, we used the GTP analog GMPPNP, which blocks initiation before the two ribosomal subunits can join, leading to a buildup of 48S ribosomal complexes[43]. Rather, the effect of Giro was consistent with translation elongation inhibition, which stalls ribosomes in the middle of open reading frames (ORFs).

To obtain a global view of ribosome traversal along ORFs, we conducted ribosome (or monosome) profiling, a deep sequencing-based method for ribosome footprints generated by RNase digestion[14], on Giro-treated HEK293T cells. In view of potential ribosome stalling by the compound, we also employed disome profiling, which

sequences the mRNA fragments protected by two closely adjacent ribosomes caused by slow elongation of the leading ribosome[15–18]. Both monosome and disome footprints were increased at the 5′ ends of the ORF (Fig. 1d), while the population around the stop codon was reduced in the disome population (Fig. 1e). This suggested increased stalling towards the 5′ ends with fewer ribosomes reaching the stop codon. We noted that there was no indication of stop-codon read-through (Fig. 1e), which contradicts earlier reports of Giro interfering with translation termination[4].

More quantitatively, we calculated the polarity score of footprint reads, a value indicating whether the average read distribution shifted towards the 5′ end (negative) or the 3′ end (positive)[36]. As expected, we saw a polarity score shift toward the 5′ end in both monosome and disome profiling (Fig. 1f, g). These data indicate that Giro does not completely block translational activity, though the observed decrease in protein output may stem from increased ribosomal stalling.

Sequence-selective stalling

In addition to the global effect of Giro on elongation, we investigated whether ribosomal stalling occurred on a particular sequence element. Therefore, we focused on the disome profiling data and analyzed the overrepresentation of individual amino acids in the ribosomal A, P, and E-sites (Fig. 2a). In the ribosomal P-site, Pro (P) and Phe (F) appeared to increase while Gln (Q), Glu (E) and especially Lys (K) were overrepresented in the E-site. This overrepresentation was also observed in our monosome data (Supplementary Fig. 1a). Analysis for disome-enriched or depleted amino acids further narrowed down the sequence context for Giro-mediated ribosome pausing. Both 1 and 10 μM Giro led to similar sequence enrichment: Lys/Pro-Pro-Pro and Lys/Pro-Phe-Pro across E, P, and A-sites (Fig. 2b). We then considered dipeptide motifs occupying either E and P-site or P and A-site together. High disome occupancy in E and P-site containing di-amino acid pairs Lys-Pro and Lys-Phe further underlined the importance of these sequences for Giro's activity (Fig. 2c). In a similar manner, we observed a significant increase of di-amino acid motifs containing P-site Pro when considering P and A-site occupancy under Giro treatment, including Pro-Pro. Disome formation on an individual Lys-Pro site inside the COX6C ORF exemplifies the context specificity of Giro (Fig. 2d). The mapped monosome data along the COX6C mRNA also shows a decrease of ribosome density toward the 3′ end.

Given the enrichment of Lys in the E-site, we wondered whether Giro would show a preference for one of the two Lys codons (AAA or AAG) in inducing ribosomal stalling. Intriguingly, we found a more pronounced increase in E-site AAA than AAG for disome formation (Fig. 2e). Sequence enrichment analysis for E-site AAA or AAG-codons (Supplementary Fig. 1b) led to the same conclusion. This was further highlighted by the disome occupancy of E and P-site with di-codon pairs, such as AAA-CCU (Lys-Pro), AAA-UUU (Lys-Phe), and AAA-CCG (Lys-Pro) (Fig. 2f). Moreover, unbiased motif analysis also showed enriched AAA, but not AAG, in the E-site (Supplementary Fig. 1c). The observed sequence-selectivity in ribosomal stalling appears to be a unique property of Giro and does not seem to result from general translation inhibition. When reducing translational output to about 40% by application of either 1 μM CHX or 0.01 μg/ml of ANS, which recapitulates the reduction in translation seen under 10 μM Giro, (Supplementary Fig. 2a, b), we did, in contrast to Giro, not observe any significant bias for either Pro or Lys in the ribosomal E, P and A-sites (Supplementary Fig. 2c, d).

Displacement of eIF5A

We were furthermore intrigued by the increase in P and A-site Pro. Increased stalling on poly-Pro motifs is usually associated with insufficient levels of the translation factor eIF5A[18,23,24,36] (Supplementary Fig. 3a, b). In addition, an increase in E-site Lys upon eIF5A depletion has previously been reported in yeast[25]. An involvement of eIF5A appeared possible since the Giro binding site on the large ribosomal subunit of *Haloarcula marismortui* is known to lie in the vicinity of where eIF5A and the ribosome interact in eukaryotes (Supplementary Fig. 3c)[10,44]. Furthermore, the binding site sits in an area of high sequence homology between archaea and eukaryotes (Supplementary Fig. 3d), making binding in the same position on ribosomes of both phyla likely.

To determine whether Giro binding affected the interaction between eIF5A and the ribosome, we used Flag-tagged eIF5A for pull-down experiments. Tagged wild-type eIF5A did pull down ribosomes, as shown by Western blotting for small and large ribosomal subunit proteins, while the hypusine-deficient Lys50-to-Ala (K50A) mutant of eIF5A did not seem to interact with the ribosome (Fig. 3a). As most overexpressed eIF5A was reported to remain non-hypusinated[45], we co-expressed DHS and DOHH, which are responsible for the generation of dehydroxyhypusine and then hypusine on Lys 50[26,27], together with tagged eIF5A. Giro was able to interfere with the binding of eIF5A to the ribosome (Fig. 3a). It furthermore blocked binding in a dose-dependent manner (Fig. 3b). While we did observe a consistent decrease in eIF5A binding in the presence of Giro, neither CHX nor ANS significantly reduced the amount of bound ribosome (Supplementary Fig. 3e), suggesting that the effect of Giro on eIF5A binding is not due to general translation inhibition.

In addition, we conducted in vivo polysome analysis and also observed an increase in the polysome population, though 80S ribosomes appeared depleted while the 40S and 60S populations also increased. The depletion of 80S ribosomes would be consistent with Giro slowing translation elongation, increasing the number of ribosomes per mRNA. It is noteworthy that, when fractionating our in vivo polysome profiles and measuring eIF5A content and ribosome distribution by Western blotting, we found that the increased polysome fraction did not contain much eIF5A (Fig. 3c).

We queried whether Giro treatment induced ribosomal pausing in the same vicinity as pausing caused by eIF5A depletion (eIF5A-KD) on an individual gene level (Fig. 3d–f) and across all significant pause sites (Fig. 3e). When we compared disome footprint distribution between Giro-treated cells and cells with RNAi-depleted eIF5A, we found in many transcripts, such as ATP5B, COX7A2, and NDUFC1 that Giro application produced ribosomal stalling in the exact same location as eIF5A depletion (Fig. 3d). Metagene analysis corroborated this finding (Fig. 3e). Focusing on significant pause sites detected under 10 μM Giro treatment, we mapped pause sites induced by eIF5A depletion 30 nucleotides upstream and downstream of the Giro-induced stall site. Both Giro treatment and eIF5A depletion caused stalling in almost the same position, though with slight differences. eIF5A depletion showed a number of smaller peaks 3′ of the main pause site.

In a few other instances, Giro caused stalling at different codons than the eIF5A-knockdown-induced stall sites (Fig. 3f). Such was the case for PPT1 and RPL38, where Giro-induced stalling occurred 5′ of the eIF5A-KD pause site. We assume that translation in the vicinity of stall sites proceeds at a slower pace. In those regions, Giro's selectivity for AAA-codons may cause the main stall site to appear in a different location than observed under eIF5A depletion. As can be seen in the sequence of the individual stall sites, Giro did not always induce stalling on AAA-codons. Rather, it seemed to prefer areas where some stalling occurs naturally, as seen by a small number of disome footprints present even in the absence of external perturbation. This was supported by comparing the stall sites between Giro treatment and eIF5A-KD with their respective controls (Supplementary Fig. 3f).

AAA-selective stalling on reporter transcripts by Giro

To test whether we could replicate stalling on AAA-encoded Lys and confirm eIF5A involvement, we utilized fluorescent FACS reporter constructs, encoding enhanced green fluorescent protein (EGFP) and red fluorescent protein (RFP) connected by a short linker sequence[46]. The linker was flanked by P2A sites[47], which allowed the ribosome to

https://doi.org/10.1038/s41467-024-54838-2

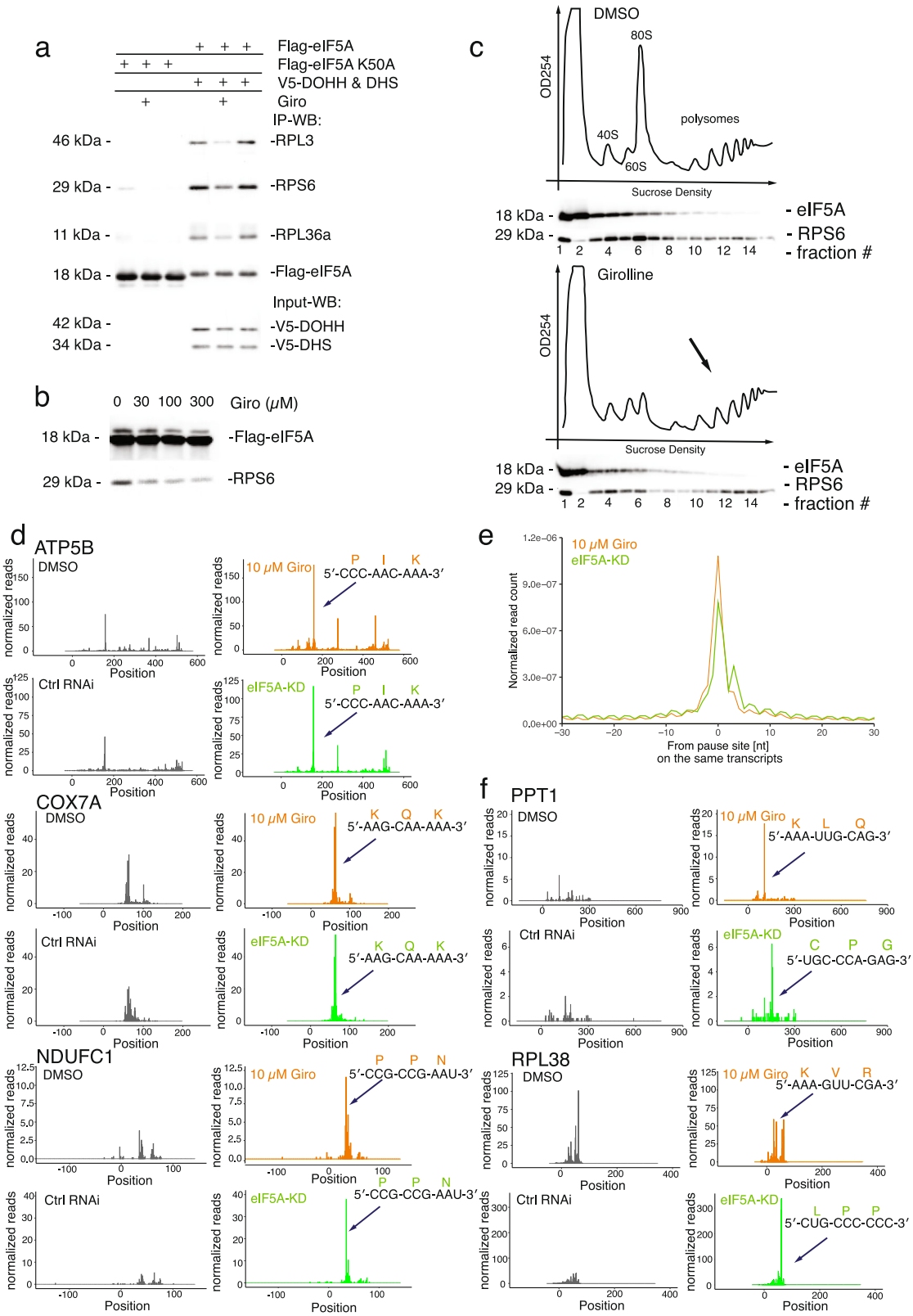

proceed on the mRNA in-frame without amino-acid incorporation. Therefore, the reporter produces three separate polypeptides from one transcript: EGFP as an internal control, the linker, and RFP as an experimental readout (Fig. 4a)[46]. If translation stalls on the linker, less RFP is produced. Cells were transfected with vector constructs 48 h before cell sorting and treated with 1 μM Giro for the last 16 h. We used an empty linker [denoted as $(XXX)_0$] for control and, as expected, did not see any effect of Giro on either EGFP or RFP expression (Fig. 4b). Then we proceeded with a linker sequence containing twenty consecutive lysines encoded by $(AAA)_{20}$ or $(AAG)_{20}$ respectively (Fig. 4c, d). Twenty AAA-codons in a row induced translational stalling with a modest reduction in RFP output compared to empty linker control, as reported previously[46]. However, Giro treatment significantly reduced RFP production further (Fig. 4c). In many cases, RFP

Fig. 3 | Giro interferes with ribosome-eIF5A interaction. a Affinity pulldown. Flag-tagged eIF5A was used to pull down ribosomes in the presence or absence of Giro. Hypusine-deficient mutant eIF5A K50A was used as a negative control. Hypusinating enzymes DOHH and DHS were co-expressed with Flag-tagged wild-type eIF5A. Ribosome pulldown was measured by Western blotting (IP-WB) against ribosomal proteins RPS6, RPL36A and RPL3. Expression of hypusinating enzymes DOHH and DHS was confirmed by Western blotting on the whole cell lysate input fraction against the V5-tag on a separate membrane (Input-WB). Expression of the K50A mutant appeared stronger than wildtype for unknown reasons. **b** Flag-pulldown of ribosomes at increasing Giro concentrations. **c** In vivo polysome profiling. Cells were treated with DMSO control or 50 μM Giro for 1 h, and lysates were centrifuged through a sucrose gradient. RNA content was monitored by OD_{254}. Key ribosomal populations are labeled in the DMSO control sample. Fractions were collected for Western blotting and probed for the presence of eIF5A and ribosomal protein RPS6. Fraction numbers are indicated below. Western blotting data is representative of at least two independently conducted experiments. **d** Disome footprints of 10 μM Giro treated (orange) or eIF5A-KD (light green) cells and their respective controls mapped across the ORFs of ATP5B, COX7A, and NDUFC1. The main disome peak is marked by an arrow with the mRNA and amino acid sequences across ribosomal E, P, and A-sites indicated. **e** Metagene analysis of significant pause sites. Genes with significant Giro-induced pause sites (1 standard deviation above the mean for reads in each gene) were probed for the location of pause sites under eIF5A depletion with their normalized reads plotted within −30 and 30 nucleotides of the Giro-induced stall site. **f** Disome footprints as in **d** where the Giro-induced stall site occurred 5′of the eIF5A-KD stall and contained AAA-encoded Lys in the E-site. Source data are provided within the Source Data file.

levels were reduced but not completely depleted, visible in the FACS profile as the filling in of the "valley" between RFP negative cells and cells with high RFP expression (arrow). Giro affected only the expression of RFP when preceded by the $(AAA)_{20}$-linker, while it had no discernible effect on a linker containing 20 consecutive AAG-codons (Fig. 4d). Furthermore, on a shorter version of the linker containing only 12 AAA-codons, 1 μM Giro had very little effect while stronger reduction of RFP production required a 5 μM dose (Supplementary Fig. 4a). This corroborated our suspicion that Giro requires a slowdown in translation to act and 20 AAA-encoded lysines seem to cause more slowing than 12. These data suggest that Giro presents a sequence context-dependent translation modulator, with a preference for ribosomal stalling on AAA-encoded Lys.

Poly-A stretches are known to induce significant amounts of frameshifting[48]. To ascertain that the observed reduction in RFP output was not the result of Giro enhancing a shift in the reading frame, we repeated the experiment with our $(AAA)_{12}$ and $(AAA)_{20}$ reporter vectors after adding one or two G-nucleotides before the 3′ P2A site. All four vectors did produce detectable RFP signals, indicating that frameshifting did occur, but the application of Giro did not lead to any visible increase compared to solvent control (Supplementary Fig. 4b). On the contrary, we could observe a decrease in RFP signal, similar to the data obtained from our in-frame vectors. Therefore, Giro did not appear to affect ribosomal frameshifting on poly-A stretches.

We then assessed eIF5A involvement, testing our FACS vectors in cells with RNAi-reduced levels of eIF5A. On cells transfected with non-targeting siRNA, Giro showed the same reduction in RFP expression observed in non-transfected cells (Fig. 5a). Even in the absence of Giro, eIF5A knock-down cells showed reduced RFP production on reporters containing the $(AAA)_{20}$-linker (Fig. 5b). The FACS profiles of eIF5A-depleted cells are virtually indistinguishable from cells with normal levels of eIF5A after treatment with 1 μM Giro (c.f. Fig. 4c). Treating eIF5A knockdown cells with Giro further reduced RFP expression, likely by preventing residual eIF5A from interacting with the ribosome (Fig. 5b). eIF5A depletion only affected the translation of the $(AAA)_{20}$-linker; using the $(AAG)_{20}$ construct, eIF5A depletion did not lead to detectable changes in RFP output (Fig. 5c, d).

We were able to replicate our key findings in vitro, utilizing a purified translation system[49–51]. An N-terminal *Renilla* luciferase (Rluc) was linked with 8 consecutive AAA-codons to a C-terminal firefly luciferase (Fluc) (Supplementary Fig. 5a). Without the addition of eIF5A, we detected only Rluc activity (Supplementary Fig. 5b). However, after eIF5A supplementation, Fluc activity was observed, indicating that eIF5A is also required in vitro to navigate poly-A sequences (Supplementary Fig. 5b, c, black line) corroborating our cell-based FACS assay data (Figs. 4 and 5). Under these conditions, in the presence of eIF5A, Giro suppressed Fluc production, confirming it counteracts eIF5A (Supplementary Fig. 5c). Giro mildly inhibited or delayed expression of the N-terminal Rluc when eIF5A was absent (Supplementary Fig. 5b), indicating that the molecule has some inhibitory activity on its own, probably through interaction with ribosomes that slowed down without eIF5A. These data suggest that Giro competes with eIF5A for ribosomal binding.

Premature translation termination by RQC activation

The FACS reporters used in this study were originally designed for research on ribosome-associated quality control (RQC) and a recent study provided some evidence for eIF5A involvement in the RQC pathway[52]. RQC triggers when the cell detects collided ribosomes via the E3 ubiquitin ligase ZNF598 and then via the ATPase ASCC3[53]. It involves separating the ribosomal subunits and destroying the nascent peptide by ubiquitination through the Ltn1 E3 ligase and the addition of non-templated alanine and threonine amino acids to the peptide's C-terminus by NEMF, known as CAT-tailing[54]. Translation of poly-A tails in mammalian cells constitutes an established way of inducing RQC.

This led us to investigate the effect of Giro on RQC induction. We modified our FACS reporter (Fig. 4a) to monitor premature translation termination and ribosomal stalling (Fig. 6a). We deleted the N-terminal P2A site and added a stop codon to the end of the linker. This construct now produced EGFP with a C-terminal tail sequence, consisting of either 20 AAA-codons or 20 GAA codons. If translation was to proceed unimpeded, we expected to see a full-length band of ~48 kDa. Stalling and premature termination would produce a shortened protein, detectable by Western blotting against EGFP. As expected, control cells showed some level of stalling made worse by the addition of Giro (Fig. 6b), indicated by an increase in the detectable proteins smaller than 48 kDa.

eIF5A knock-down itself (Supplementary Fig. 6a) led to an increase of these shortened proteins similar to treatment with 1 μM Giro (Fig. 6b). This further corroborated that eIF5A aids the translation of poly-A stretches.

When RQC trigger factors ASCC3 or ZNF598 were knocked down (Supplementary Fig. 6a), Giro lost its effect, and translation proceeded to full length (Fig. 6b). The translational complexes stalling on a poly-A sequence should still be translation-competent and proceed to the end of the reading frame by themselves if RQC does not engage. When downstream RQC factors Ltn1 and NEMF were depleted, more stalled proteins accumulated, possibly because depletion of these factors slows down the clearance of stalled nascent peptides (Fig. 6b). Importantly, prematurely terminated peptides were only observed on the $(AAA)_{20}$ construct, while the translation of $(GAA)_{20}$ or $(AAG)_{20}$ did complete unimpeded, irrespective of Giro treatment or RQC factor knockdown (Fig. 6c and Supplementary Fig. 6b). It is known that the AAA-codon presents more challenges to the translation machinery than AAG and thus acts as a RQC substrate[48,55]. This appears due to adenosine nucleotides potentially forming single-stranded helices, interfering with decoding[55,56], while the positively charged Lys can interact with the negatively charged rRNA around the peptide exit tunnel, including an interaction between the second (E-site) amino acid in the nascent peptide, which pulls the P-site tRNA into a less productive conformation for the next peptidyl transfer[56]. Part of Giro's cytotoxicity may stem not

https://doi.org/10.1038/s41467-024-54838-2

from translational inhibition alone but from premature activation of the RQC pathway, as knockdown of ASCC3 conveyed some resistance to Giro treatment (Supplementary Fig. 6c, d).

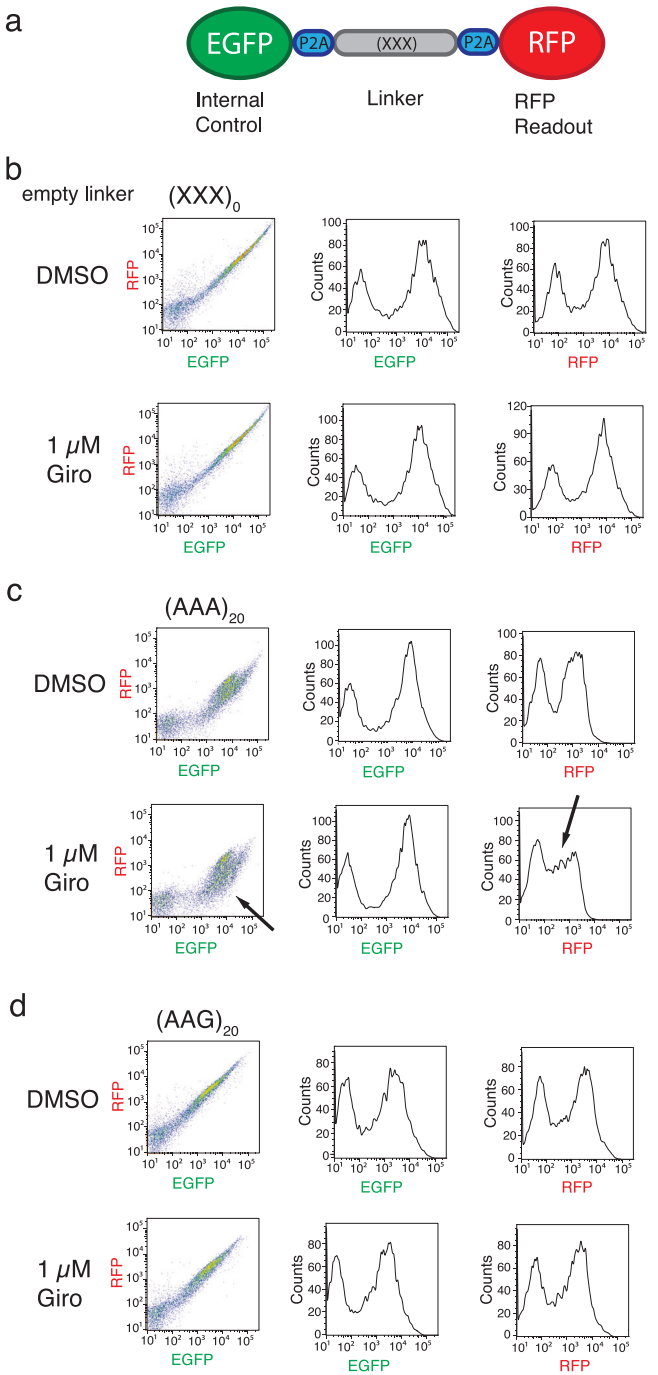

Fig. 4 | Sequence-selective stalling on FACS reporters. a FACS reporter used in this study. The vector produces three peptides from one transcript: EGFP as internal control, linker, and RFP as experimental readout. The linker sequence was varied for each set of experiments. Cells were transiently transfected with the reporter vector before overnight treatment with DMSO control or 1 μM Giro **b** Control readout for the empty linker $(XXX)_0$. Graphs indicate the RFP signal plotted against EGFP and the histograms of EGFP and RFP signal respectively. The left peaks in each histogram indicate non-fluorescing cells. **c** FACS readout for a vector containing a linker of 20 consecutive AAA-Lys codons $(AAA)_{20}$ in the presence of DMSO or 1 μM Giro. Arrows in the Giro sample highlight cell populations with low levels of RFP production. **d** FACS readout as above but for vector containing 20 consecutive AAG-Lys codons $(AAG)_{20}$. Data for each condition are representative of at least 3 independently carried out experiments. Gating information is available in Supplementary Fig. 8.

Discussion

In this study, we provide evidence that Giro is a sequence-selective modulator of eIF5A function. We have shown that in the presence of Giro, eIF5A binding to the ribosome decreases (Fig. 3a, b). Furthermore, we have demonstrated that Giro treatment and eIF5A depletion lead to ribosomal stalling in largely the same locations (Fig. 3d, e). Both Giro and eIF5A-KD caused stalling on poly-Pro motifs (Fig. 2a, b, and Supplementary Fig. 3b), while Giro further underlined the need for eIF5A in translating lysine, previously observed in yeast. We could demonstrate through FACS reporter assays that eIF5A is required for the translation of poly-A stretches and could replicate this finding in vitro (Fig. 5 and Supplementary Fig. 5). In addition, we found evidence for eIF5A preventing premature activation of the RQC pathway and saw that part of Giro's cytotoxicity stems from RQC activation (Fig. 6 and Supplementary Fig. 6). Giro does appear to inhibit translation by itself (Supplementary Fig. 5), though this aspect appears more pronounced in vitro than in cellular assays and might be explained by increased Giro-susceptibility through slowed translation in the absence of eIF5A.

Our data supports the following model (Fig. 7). On sequences where translation slows down, including stretches with positively charged amino acids, poor decoding, and slow peptidyl transfer, eIF5A is required to maintain translation elongation to prevent slowing ribosomes from stalling (Fig. 7a). Slow translation provides an opportunity for Giro to bind around the ribosomal E-site. This likely occurs when slow decoding and peptidyl transfer leave the E-site empty for longer than usual after the release of the deacylated tRNA. Giro binding prevents eIF5A from aiding the next round of peptidyl transfer (Fig. 7b), thereby turning slowing into stalling. The stalled ribosomes are then detected and disposed of by the RQC pathway. This mode of action may bear some resemblance to that of lactimidomycin[57], which only inhibits translation during the first round of elongation but is unable to compete with deacylated tRNA for the ribosomal E-site when the ribosome is actively translating.

This model would support eIF5A's involvement in a wide range of challenging sequence contexts[23,36,58], guarding protein synthesis against premature activation of quality control mechanisms. The observed increase in polysomes and 40S and 60S ribosomal subunits in our polysome profiling data (Fig. 3c) would agree with an increase in split ribosomal subunits owing to heightened RQC activity.

Translational slowing appears to be key for Giro activity, and, physiologically, translation speed depends on a wider sequence context. Our cellular ribosome profiling data highlighted increased stalling on Pro-containing sequences and E-site Lys, though this does not mean that stalling is exclusive to these sequences (c.f. Fig. 3d). While our FACS reporters are limited and do not account for processes such as co-translational processing or protein import into organelles, we were able to dissect out some aspects of the sequence context in which Giro acts. Charged amino acids preceding the stall site appear to play an important role in sensitizing ribosomes to Giro. This notion can be corroborated by our disome profiling data. We calculated the average isoelectric point (pI) for the amino acids in the nascent peptide chain of our disome fraction as a measure of positive charge. We noticed an increase in average pI about 4 to 7 amino acids upstream from the A-site (Supplementary Fig. 7a, b). This effect was even more pronounced when only considering the Giro-stalled disome fractions containing AAA in the E-site (Supplementary Fig. 7c). The combination of an element, such as a positive charge, causing slowing ahead of a stall site may explain why, in the context of our FACS vectors, we did not observe significant stalling on a stretch of 20 Pro residues (Supplementary Fig. 7d, e).

We cannot completely rule out that Giro acts as a weak general translation inhibitor, whose action only happens to coincide with a requirement for eIF5A. However, this seems unlikely, since weak general translation inhibition does not produce a sequence bias for Pro or

https://doi.org/10.1038/s41467-024-54838-2

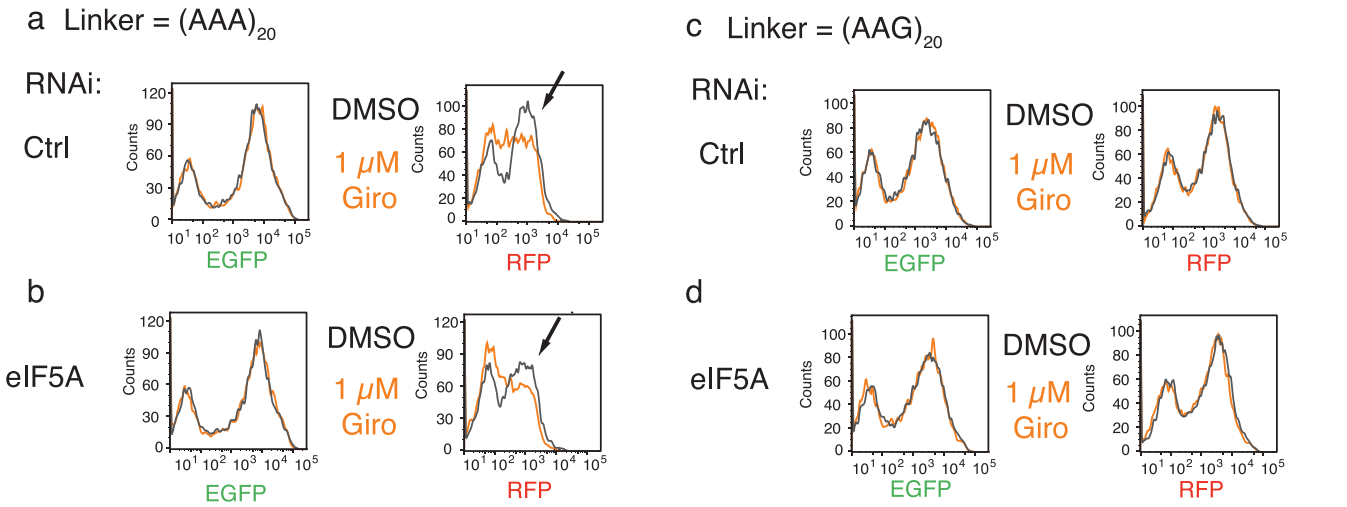

Fig. 5 | eIF5A is required for unimpeded AAA translation. a, **b** Overlay of EGFP and RFP histograms for a non-targeting siRNA pool **a** and eIF5A-KD **b** treated with 1 μM Giro on the $(AAA)_{20}$ reporter. **a** Histograms of EGFP and RFP expression in control RNAi pool cells upon 1 μM Giro (orange) or DMSO control (black) treatment (c.f. Figure 4c). **b** Histograms of EGFP and RFP expression in cells with depleted eIF5A in the presence or absence of 1 μM Giro. Arrows highlight the peak of RFP expression in cells treated with DMSO control for cells transfected with non-targeting siRNA **a** or eIF5A-KD **b**. **c**, **d** EGFP and RFP histograms for non-targeting RNAi pool **c** or eIF5A-KD **d** in the presence or absence of 1 μM Giro on the $(AAG)_{20}$ reporter. Data is representative of at least three independently conducted experiments. Gating information and histograms are available in Supplementary Fig. 8.

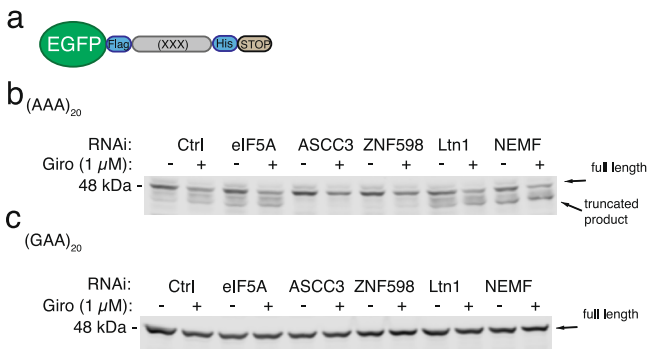

Fig. 6 | Giro induces RQC. a Adjusted reporter construct for Western blotting. The N-terminal P2A site was deleted, and a stop codon was added to the end of the linker. **b** Western blot against EGFP for cells depleted in eIF5A and key factors in ribosome quality control, each treated with DMSO or 1 μM Giro and transfected with $(AAA)_{20}$-reporter. Arrows indicate full-length protein of ~ 48 kDa and truncated products **c** western blot against EGFP for cells depleted in eIF5A or RQC factors and expressing a $(GAA)_{20}$ -reporter. Data is representative of three independently conducted experiments. Source data are provided within the Source Data file.

Lys, nor does it lead to decreased eIF5A interaction with the ribosome (Supplementary Fig. 2 and 3e). In fact, other studies indicate that CHX binding to the ribosome enhances the association between ribosome and eIF5A[59,60]. Although eIF5A-depletion did not render cells more sensitive to Giro application (Supplementary Fig. 6f, g), as eIF5A is a highly expressed protein, the reduction in protein level by ~ 70% during RNAi treatment may not suffice to visibly reduce cell viability in cultured conditions. Also, the large overlap between ribosome stall sites in the presence of Giro or absence of eIF5A (Fig. 3d, e) would argue in favor of a direct effect of Giro on eIF5A activity, as does the similar behavior of ribosomes on poly-A stretches under Giro treatment or eIF5A-KD (Fig. 5 and Supplementary Figs. 5, 6). Future structural studies and a refined understanding of the wider sequence contexts favoring ribosomal slowdown should help resolve remaining ambiguities in Giro's mechanism of action.

Sequence-selective inhibition of translation elongation by small molecules has been observed in a number of cases[61–64]. However, the molecules reported so far seemed to act on the peptide exit tunnel side of the peptidyl transfer center[62,63,65], via the ribosomal A-site[61] or even the 30S subunit[64]. This makes Giro's activity around the large subunit's E-site unique.

Knockdown of ASCC3 and ZNF598 overcame ribosomal stalling on poly-A sequences, underlining that reduced protein output and premature termination on the $(AAA)_{20}$-sequence were due to RQC involvement. A recent structural study identified eIF5A as part of RQC complexes and suggested that it plays a role in peptide formation during CAT-tailing[54]. It is important to consider that this involvement of eIF5A takes place after the ribosomal subunits have been split apart. Our data suggest that, while translation is in progress, eIF5A prevents RQC activation.

In terms of a wider physiological context, the observed involvement of eIF5A in aging and the maintenance of mitochondrial health[66,67] may not be the result of one particular protein not being properly expressed, but rather a "death by a thousand cuts", with decreasing translational efficiency leading to increased stalling, premature processing by the RQC machinery and a slowly deteriorating proteome. The observed increase in resistance to Giro upon ASCC3 depletion would support this notion.

We expect Giro to become a useful tool compound for triggering RQC and for globally modulating eIF5A function in various physiological settings. Given the difficulty in genetically manipulating eIF5A due to its lethality, we think that Giro will be of particular interest in the study of eIF5A involvement in aging and neurodegeneration.

Despite its known effect on cancer cell proliferation, Giro's therapeutic potential has not been comprehensively explored. It did enter clinical trials against neoplasms in the past, though they seem not to have advanced past phase I, owing to dose-limiting toxicity and lack of observed anti-tumor effect[68]. Perhaps more intriguing is the reported anti-malarial activity. *Plasmodium falciparum* mRNAs are AT-rich and carry poly-A stretches in their coding regions[69]. Our findings finally provide a mechanistic explanation for Giro's toxicity against *Plasmodium*. Given the enormous societal toll malaria still exacts, Giro should be re-evaluated for its potential in anti-parasitic therapy. It is possible that sequence context-selective inhibition of protein synthesis provides sufficient specificity to offer a therapeutic window for Giro to be explored as an antimalarial agent. We are therefore confident that Giro

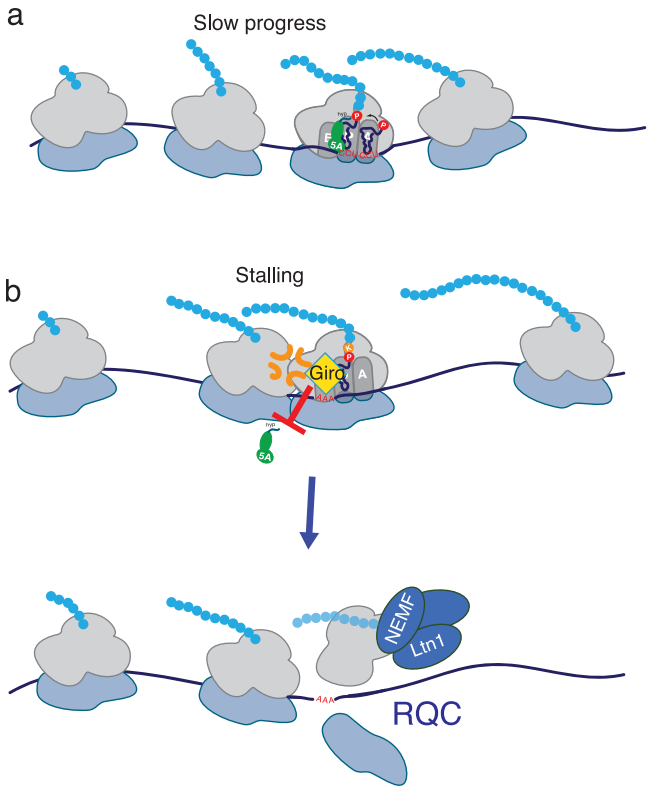

Fig. 7 | Model of Giro- and eIF5A-mediated translational modulation. a On sequences slowing translation, including but not limited to poly-Pro, eIF5A is required to expedite translation elongation. **b** Slowed translation enables Giro binding to the ribosome, preventing eIF5A from aiding peptidyl transfer, thereby turning ribosomal slowing into ribosomal stalling and subsequent collision with the following ribosome. This prematurely activates the ribosome-associated quality control pathway (RQC), which splits the ribosomal subunits apart and initiates the destruction of the nascent peptide.

will prove a useful chemical probe for research on translation, aging, mitochondrial health and beyond.

Significance

We present a sequence context-selective modulator of eIF5A activity, which prevents the interaction between its target protein and the large ribosomal subunit and induces ribosomal stalling, including on Pro-containing sequences and AAA-encoded Lys. We demonstrate that eIF5A ensures speedy translation and plays a role in preventing the premature degradation of nascent peptides by the ribosome-associated quality control pathway. Our results indicate that Giro has the potential as a chemical probe to understand the role of eIF5A in a wide variety of physiological contexts and may provide a basis for the development of further sequence-selective translation modulators.

Methods

Tissue culture

HEK293 Flp-In T-Rex cells (Thermo Fisher Scientific, R78007), HEK293T cells and HeLa S3 cells (gift from Prof. Fumio Hanaoka, University of Tokyo) were grown at 37 °C and 5% CO_2 in DMEM high glucose medium with glutamine (Wako), supplemented with antibiotics and 10% fetal bovine serum.

Compounds

Giro (isolated by Drs. Ali Al Mourabit and Celine Moriou, provided by Dr. Daniel Romo) was dissolved in DMSO to 100 mM stock concentration and stored at − 30 °C.

Flag-tag pulldowns

The ORFs of human eIF5A, DOHH, and DHS were amplified from reverse-transcribed Hela cell mRNA and cloned into pcDNA3.1 vectors with N-terminal Flag or V5 tags. Flag-tagged wildtype eIF5A or the eIF5A K50A mutant were overexpressed in HEK293T cells with or without V5-tagged DHS and DOHH. After 24 h, cells were treated with DMSO solvent control, 10 μM and 100 μM Giro or 1 μM and 10 μM CHX or 0.01 μg/ml and 0.1 μM ANS for 1 h and lyzed in TMK100 buffer (20 mM Tris-HCl pH 7.4, 100 mM KCl, 5 mM $MgCl_2$, 2 mM DTT, 1% Triton-X 100, 100 μ/ml RNasIN in DEPC RNase free water). Identical amounts of lysate were incubated with 30 μl Flag M2 antibody-conjugated agarose beads (Sigma) for 1 h. After 3 washes with TMK100 buffer, beads were boiled in 80 μl 1x Laemmli loading buffer and separated by SDS-PAGE for Western blotting and silver or Coomassie brilliant blue staining. Data is representative of at least 3 independently conducted experiments.

RNAi

Cells were plated in 6-well format at 500.000 cells per well overnight, treated with 90 pmol RNAi constructs (Dharmacon ON-TARGETplus siRNAs) against eIF5A1 (L-015739-00-0005), ASCC3 (L-012757-01-0005), ZNF598 (L-007104-00-0005), LTN1 (L-006968-00-0005), NEMF (L-019106-02-0005), or non-targeting control (D-001810-10-05) using Thermo Lipofectamine RNAiMax according to the manufacturer's instructions, and incubated for 72 h before analysis. Knockdown was confirmed by Western blot.

Cytotoxicity

Cells were plated out and transfected with RNAi constructs as stated above. 24 h after transfection, cells were plated out at 20,000 cells/well in 96-well format and allowed to adhere for 6 h. An aliquot of 1.3 million cells was retained in 6-well format and grown till the termination of the experiment before being lysed in 300 μl of Laemmli loading buffer for Western blot confirmation of knockdown efficiency. Giro was added to the cells in the 96 well plates at 20, 10, 5, 1, 0.5, 0.1, 0.05, and 0.01 μM or DMSO solvent control. Cells were then allowed to grow for another 40 h before the addition of 10 μl WST-8 reagent (Nacalai Cell Count SF) per well for 4 h. Optical density at 450 nm was then measured with background deduction on a Biorad Plate reader. Data present two independent replicates, measured in quadruplicate and processed with GraphPad Prism software for normalization and curve fitting.

FACS analysis

Cells seeded in 6-well plates were transfected with 2 μg plasmid DNA [either pmGFP-P2A-K0-P2A-RFP (Addgene plasmid # 105686; http://n2t.net/addgene:105686; RRID:Addgene_105686), pmGFP-P2A-K(AAA)12-P2A-RFP (Addgene plasmid # 105687; http://n2t.net/addgene:105687; RRID:Addgene_105687), pmGFP-P2A-K(AAA)20-P2A-RFP (Addgene plasmid # 105688; http://n2t.net/addgene:105688; RRID:Addgene_105688) or pmGFP-P2A-K(AAG)20-P2A-RFP (Addgene plasmid # 105689; http://n2t.net/addgene:105689; RRID:Addgene_105688); gifts from Ramanujan Hegde] and 8 μl X-tremeGENE HP (Roche), incubated for 24 h, and then treated with compounds at the indicated concentrations for 16 h. Cells were washed once with cold PBS, trypsinized, and quenched with PBS containing 10% fetal bovine serum. Cell suspensions were then pipetted into 5-ml round bottom polystyrene tubes with a cell strainer (Falcon, cat# 352235) and kept on ice until analysis on a FACSAria II Special Order System (BD). Each experiment was carried out at least three times, and representative examples were chosen for illustration in the figures. Gating information is provided in Supplementary Fig. 8.

DNA construction

pmGFP-P2A-K(AAA)20-P2A-RFP was modified for use in western blotting[70]. The P2A sequence between the EGFP and 3xFLAG sequence in the pmGFP-P2A-K(AAA)20-P2A-RFP vector (addgene plasmid

#105688) was deleted by site-directed mutagenesis using the PrimeSTAR® Mutagenesis Basal Kit (Takara, R046A).

Forward primer: gcagcggcggtactgactacaaagaccatgacg

Reverse primer: cagtaccgccgctgcctccggacttgtacagct

(AAA)20-His-Stop, (GAA)20-His-Stop, and (AAG)20-His-Stop genes were inserted into the vector after cutting with Sal I and Kpn I using the Mighty mix (Takara, 6023) for ligation. The gene fragments were purchased as synthetic genes from Eurofins Genomics.

(AAA)20-His-Stop:

cgccatggcgaccaaaaaaaaaaaaaaaaaaaaaaaaaaaaaaaaaaaaaaaaaaaaaaaaaaaaaaaaaaaaaaaaaaaaaaaggtggtcatcatcattagcccgggggatcc

(GAA)20-His-Stop:

cgccatggcgaccgaagaagaagaagaagaagaagaagaagaagaagaagaagaagaa-gaagaagaagaagaagaaggtggtcatcatcattagcccgggggatcc

(AAG)20-His-Stop:

cgccatggcgaccaagaagaagaagaagaagaagaagaagaagaagaagaagaagaa-gaagaagaagaagaagaagggtggtcatcatcattagcccgggggatcc

The fragments were modified to include the Sal I recognition sequence at the 5' end and the Kpn I recognition sequence at the 3' end. A Vector map is provided in Supplementary Fig. 9.

Polysome profiling

Polysome profiling was carried out as before[57,71]. Briefly, HEK293T cells were grown close to confluency in 15 cm dishes. 50 μM Giro or DMSO solvent control was applied for 60 min. Cells were briefly washed in cold PBS and lysed in 30 mM Tris-HCl pH 7.4, 100 mM KCl, 5 mM $MgCl_2$, 2 mM DTT, and 1% Triton-X 100. Lysates were cleared by centrifugation at 20,000 × *g* at 4 °C for 10 min. Aliquots containing the same amount of RNA normalized by OD_{254} were loaded onto 15–45% sucrose gradients and centrifuged for 90 min at 40,000 rpm in an SW41Ti swing bucket rotor (Beckman Coulter). The distribution of ribosomes was monitored by OD_{254} through an in-line spectrophotometer. Aliquots were collected for Western blotting. The experiment was carried out at thrice for reproducibility.

For in vitro polysome profiles, β-globin mRNA was reverse transcribed with T7 RNA polymerase in the presence of 1 mM ATP, CTP, UTP, and 0.5 mM GTP as well as 30 μCi α-[^{32}P] GTP and 2 mM m^7G cap analog using a commercial kit (Ribomax, Promega). An aliquot of 200 ng of radiolabeled RNA was added to 25 μl rabbit reticulocyte lysate (RRL) translation reactions supplemented with KCl, DTT, and amino acids, as described above. After incubation at 30 °C for 15 min, samples were diluted to a total volume of 200 μl in gradient buffer (20 mM Hepes-KOH pH 7.4, 100 mM KCl, 5 mM $MgCl_2$, and 2 mM DTT) and centrifuged through 15–35% sucrose gradients using an SW55Ti rotor (Beckman Coulter) at 50,000 rpm and 4 °C. 200 μl fractions were collected by hand and scintillation-counted on a Perkin Elmer Microbeta luminometer.

Labeling of newly synthesized proteins with OP-puro

The procedure was carried out as reported previously[72]. Briefly, 250,000 HEK293T cells/well were plated into 24-well plates and grown overnight. The next day, the medium was replaced with 500 μl fresh culture medium containing Giro at the indicated concentrations in triplicate. As a control, 100 μg/ml of cycloheximide (CHX) was included. Cells were incubated for 90 min before the dropwise addition of 50 μl Opti-MEM containing 200 μM *O*-propagyl-puromycin (OP-Puro, Jena Bioscience). Cells were incubated for a further 30 min before washing with 500 μl ice-cold PBS. After careful removal of the medium, cells were collected in cold 60 μl lysis buffer (20 mM Tris-HCl pH 7.5, 150 mM NaCl, 5 mM $MgCl_2$, and 1% Triton-X 100) by pipetting up and down, followed by 10 min incubation on ice. The lysate was cleared by centrifugation at 20,000 × *g* for 10 min at 4 °C. Fifteen microliters of lysate were reacted with 0.4 μl of 50 μM IRdye800CW (LI-COR Biosciences) using a Click-it cell reaction kit (Thermo Fisher Scientific) according to the manufacturer's instructions and incubated at 25 °C for 30 min. Meanwhile, G-25 gel filtration columns (Cytiva) were washed thrice with 500 μl lysis buffer containing 1 mM DTT by centrifugation at 740 × *g* for 1 min at 4 °C.

The click reaction was then loaded onto the washed columns and spun at 740 × *g* for 2 min at 4 °C. The eluted lysate was mixed with 6 μl of 6 × IR-compatible loading buffer (LI-COR Biosciences) and heated to 95 °C for 5 min. Ten microliter aliquots were loaded onto a 5–20% gradient gel and resolved at a constant 20 mA current in Tris-glycine-SDS buffer. The gel was then briefly washed in MilliQ water and fixed with a 50% methanol and 7% acetic acid solution for 15 min. The gel was washed for 15 min in MilliQ water before visualizing on an Odyssey CLx (LI-COR Biosciences) through the 800 nm channel and quantitation of the signal per lane. Afterwards, the gel was stained with Coomassie by incubation with Gel Code Blue reagent (Thermo Fisher Scientific) for 30 min and then washed in MilliQ water overnight. The gel was again scanned on the Odyssey CLx scanner, and the total protein was quantified using the 700 nm channel. Data was analyzed by dividing the IR800 signal by the Coomassie signal at IR700.

Monosome profiling, disome profiling, and RNA-Seq

Lysate preparation. Library preparation was conducted as previously reported[18,73], starting with RNA isolation. Briefly, HEK293 Flp-In T-Rex cells were plated to 1×10^7 cells in 10-cm dishes overnight. Cells were treated for 2 h with either DMSO solvent control or 1 and 10 μM Giro or 1 μM cycloheximide (CHX) or 0.01 μg/ml anisomycin (ANS). DMSO, CHX, ANS, and knock-down samples were collected in independent duplicates. For eIF5A knock-down samples, cells were transfected with Dharmacon smartPool siRNA (L-015739-00-0005) using Lipofectamine RNAiMAX (Thermo Fisher Scientific) according to the manufacturer's instructions 72 h before lysis, as described earlier[18]. Knock-down efficiency was about 70% as measured by Western blotting. Cells were washed once with ice-cold PBS and then lysed in 600 μl lysis buffer (20 mM Tris-HCl pH 7.5, 150 mM NaCl, 5 mM $MgCl_2$, 1% Triton-X 100, 1 mM DTT, 100 μg/ml cycloheximide, and 100 μg/ml chloramphenicol). Lysates were digested with DNase and cleared by centrifugation. After determining RNA concentration by Qubit BR (Thermo Fisher Scientific), lysate containing 10 μg of RNA was used for each sample.

Library preparation, monosome, and disome profiling. Library preparation was continued as previously reported[73]. Briefly, the lysate containing 10 μg RNA was scaled up to 300 μl in lysis buffer, and digested with 2 μl (10 U/μl) RNase I (Epicenter) for 45 min at 25 °C. The reaction was stopped by the addition of 10 μl SUPERase•IN RNase inhibitor (Thermo Fisher Scientific) and cooling samples on ice. The digested RNA solution was then placed on a 900 μl cushion of 1 M sucrose and centrifuged for 1 h at 100,000 rpm, 4 °C in a TLA110 ultracentrifuge rotor (Beckman Coulter). The pellet was dissolved in 300 μl TRIzol reagent (Thermo Fisher Scientific), and RNA was purified using the Direct-zol RNA MicroPrep Kit (Zymo Research) according to the manufacturer's instructions. The purified RNA was then separated by gel electrophoresis on 15% denaturing acrylamide gels (Wako, SuperSep) in TBE (10x RNAse free, Promega) running buffer. For monosome analysis a gel slice ranging from 17–34 nt was excised, and for disomes from 50–80 nt. The gel slices were crushed and RNA was eluted with TE buffer (nacalai tesque, pH8) overnight. RNA fragments were purified, ligated into sequencing adapters, and rRNA-depleted using the Ribo-Zero kit gold kit, included in the TruSeq Stranded total RNA-sequencing kits (Illumina). After PCR amplification, disome libraries were cleaved with a custom gRNA and Cas9 protein as described earlier[73] to further reduce rRNA contamination.

Data analysis. Custom scripts outlining initial data processing were made public previously[74] under: doi.org/10.5281/zenodo.10644574. Data analysis was conducted as published previously[18,75,76] using the scripts

indicated above. Monosome and disome occupancies were calculated as the ratio of reads at a given codon to the average reads per codon on that transcript. Disome pause sites were defined as codons with disome occupancies larger than the mean plus 1 standard deviation. Monosonome and disome profiling data with eIF5A knockdown and the control siRNA were obtained from our previous study GSE145723[18].

Amino acids associated with ribosome stalling were illustrated with kpLogo[77]. Data obtained from DMSO solvent control or non-targeting siRNA pool was used for background deduction. pI was calculated within a 6 amino acid window of the nascent chain of the stalled ribosome using the R Peptides package.

Overlaps in the pause site were calculated by taking average disome reads from 10 μM Giro-treated cells that lay one standard deviation above the mean for reads in each gene. Disome reads from eIF5A-depleted samples were then depicted within 30 nucleotides upstream and downstream of the Giro pause sites.

Western blot. Cell lysates were collected in 1x SDS buffer (50 mM Tris-HCl pH 6.8, 2% SDS, 10% glycerol, 1% β-mercaptoethanol, 12.5 mM EDTA, and 0.02% bromophenol blue) and denatured by heating to 95 °C for 10 min. Five to fifteen microliter aliquots were run on 5–20% gradient gels in Tris-glycine-SDS buffer and then transferred onto nitrocellulose membranes (BioRad). Membranes were blocked with Intercept TBS blocking buffer (LI-COR Biosciences) for 1 h and incubated overnight with primary antibodies in Intercept TBS blocking buffer. Unless otherwise noted, antibody dilution was 1:1000. Antibodies used in this study were as follows: anti-tubulin (1:5000; SCBT, sc-23948 or 1:2500; abcam, ab52866), anti-eIF5A (BD Biosciences, 611977), anti-ZNF598 (Thermo Fisher Scientific, PA5-31410), anti-NEMF (Thermo Fisher Scientific, PA5-49768), anti-LTN1 (1:500; Thermo Fisher Scientific, PA5-42315), anti-ASCC3 (Proteintech, 17627-1-AP), anti-GFP (Abcam, ab290), anti-RPS6 (Cell Signal, S2217), anti-RPL36a (SCBT, sc100831), anti-RPL3 (SCBT, sc86826), anti-V5 (abcam, ab27671) and anti-Flag M2 (1:1000-2000; Sigma, F1804). After incubation, membranes were washed thrice in TBS-T (0.05% Tween) buffer for 15 min before incubation with a secondary antibody (anti-mouse antibody conjugated with IRDye 680CW, LI-COR Biosciences, 926-68070 or anti-rabbit antibody conjugated with IRDye 800RD, LI-COR Biosciences, 926-68071) for 1 h at 1:10,000 dilution. For Western blots developed with horseradish peroxidase (HRP)-linked secondary antibodies, blocking was carried out in TBS buffer containing 0.05% Tween and 5% milk. Membranes were incubated with a 1:2000 dilution of secondary antibody (GE ECL anti-rabbit, NA934V, or anti-mouse NA931V) and developed with Millipore Immobilon substrate (S0500).

Reconstituted in vitro translation. The in vitro reconstituted translation system with purified 40S and 60S ribosomal subunits, human translation factors, and tRNAs was used as described previously[49–51]. We used the final concentrations: cap-Rluc-3 × Flag-SBP-K$(AAA)_8$-Fluc-polyA mRNA template at 0.075 μM. 40S, 60S ribosomal subunits at 0.48 μM. Each reaction was prepared in a 28 μl volume and split into 8 μl aliquots on ice. Reactions were incubated in the presence of eIF5A and Giro at the indicated concentrations on ice for 15 min and then at 32 °C for the indicated reaction times. 6 μl aliquots from each reaction were analyzed with a Dual-Luciferase Reporter Assay System (Promega E1910) on a multimode plate reader (EnVision - PerkinElmer), and the averages were plotted. Three independent experiments were conducted; the standard deviation was calculated for each time point.

Reporting summary

Further information on research design is available in the Nature Portfolio Reporting Summary linked to this article.

Data availability

Monosome profiling, disome profiling, and RNA-Seq data obtained for Giro-treated cells are available in the GEO depository under accession number: GSE233886 [https://www.ncbi.nlm.nih.gov/geo/query/acc.cgi?acc=GSE264204], monosome and disome profiling data at low doses of CHX and ANS under accession number: GSE264204. Source data are provided in this paper.

Code availability

Custom Scripts for data analysis in this study were uploaded to Zenodo and are available at: https://doi.org/10.5281/zenodo.11277016.

References

1. Chiaroni, A. et al. Crystal-structure and absolute-configuration of girolline. *Health Eviron. Res. Online* **312**, 49–53 (1991).
2. Ahond, A. et al. Girolline, a new antitumoral compound extracted from the sponge, pseudaxinyssa-cantharella N-Sp (Axinellidae). *Cr Acad. Sci. Ii* **307**, 145–148 (1988).
3. Lavelle, F., Zerial, A., Fizames, C., Rabault, B. & Curaudeau, A. Antitumor activity and mechanism of action of the marine compound girodazole. *Invest. N. Drugs* **9**, 233–244 (1991).
4. Colson, G., Rabault, B., Lavelle, F. & Zerial, A. Mode of action of the antitumor compound girodazole (RP 49532A, NSC 627434). *Biochem. Pharm.* **43**, 1717–1723 (1992).
5. Tsukamoto, S. et al. Girolline, an antitumor compound isolated from a sponge, induces G2/M cell cycle arrest and accumulation of polyubiquitinated p53. *Biol. Pharm. Bull.* **27**, 699–701 (2004).
6. Benoit-Vical, F., Salery, M., Soh, P. N., Ahond, A. & Poupat, C. Girolline: a potential lead structure for antiplasmodial drug research. *Planta Med.* **74**, 438–444 (2008).
7. AlMourabit, A. et al. Pyraxinine, a novel nitrogenous compound from the marine sponge Cymbastela cantharella. *J. Nat. Prod.* **60**, 290–291 (1997).
8. Sauleau, P. et al. Dihydrohymenialdisines, new pyrrole-2-aminoimidazole alkaloids from the marine sponge Cymbastela cantharella. *Tetrahedron Lett.* **52**, 2676–2678 (2011).
9. Fung, S. Y. et al. Unbiased screening of marine sponge extracts for anti-inflammatory agents combined with chemical genomics identifies girolline as an inhibitor of protein synthesis. *ACS Chem. Biol.* **9**, 247–257 (2014).
10. Schroeder, S. J., Blaha, G., Tirado-Rives, J., Steitz, T. A. & Moore, P. B. The structures of antibiotics bound to the E site region of the 50 S ribosomal subunit of Haloarcula marismortui: 13-deoxytedanolide and girodazole. *J. Mol. Biol.* **367**, 1471–1479 (2007).
11. Ingolia, N. T. Ribosome profiling: new views of translation, from single codons to genome scale. *Nat. Rev. Genet.* **15**, 205–213 (2014).
12. Iwasaki, S. & Ingolia, N. T. The growing toolbox for protein synthesis studies. *Trends Biochem. Sci.* **42**, 612–624 (2017).
13. Shichino, Y. & Iwasaki, S. Compounds for selective translational inhibition. *Curr. Opin. Chem. Biol.* **69**, 102158 (2022).
14. Ingolia, N. T., Ghaemmaghami, S., Newman, J. R. & Weissman, J. S. Genome-wide analysis in vivo of translation with nucleotide resolution using ribosome profiling. *Science* **324**, 218–223 (2009).
15. Arpat, A. B. et al. Transcriptome-wide sites of collided ribosomes reveal principles of translational pausing. *Genome Res.* **30**, 985–999 (2020).
16. Meydan, S. & Guydosh, N. R. Disome and trisome profiling reveal genome-wide targets of ribosome quality control. *Mol. Cell* **79**, 588–602 (2020).
17. Zhao, T. et al. Disome-seq reveals widespread ribosome collisions that promote cotranslational protein folding. *Genome Biol.* **22**, 16 (2021).
18. Han, P. et al. Genome-wide survey of ribosome collision. *Cell Rep.* **31**, 107610 (2020).

19. Schnier, J., Schwelberger, H. G., Smit-McBride, Z., Kang, H. A. & Hershey, J. W. Translation initiation factor 5A and its hypusine modification are essential for cell viability in the yeast Saccharomyces cerevisiae. *Mol. Cell Biol.* **11**, 3105–3114 (1991).
20. Kang, H. A., Schwelberger, H. G. & Hershey, J. W. The two genes encoding protein synthesis initiation factor eIF-5A in Saccharomyces cerevisiae are members of a duplicated gene cluster. *Mol. Gen. Genet.* **233**, 487–490 (1992).
21. Kang, H. A., Schwelberger, H. G. & Hershey, J. W. Translation initiation factor eIF-5A, the hypusine-containing protein, is phosphorylated on serine in Saccharomyces cerevisiae. *J. Biol. Chem.* **268**, 14750–14756 (1993).
22. Schwelberger, H. G., Kang, H. A. & Hershey, J. W. Translation initiation factor eIF-5A expressed from either of two yeast genes or from human cDNA. Functional identity under aerobic and anaerobic conditions. *J. Biol. Chem.* **268**, 14018–14025 (1993).
23. Saini, P., Eyler, D. E., Green, R. & Dever, T. E. Hypusine-containing protein eIF5A promotes translation elongation. *Nature* **459**, 118–121 (2009).
24. Gutierrez, E. et al. eIF5A promotes translation of polyproline motifs. *Mol. Cell* **51**, 35–45 (2013).
25. Pelechano, V. & Alepuz, P. eIF5A facilitates translation termination globally and promotes the elongation of many non polyproline-specific tripeptide sequences. *Nucleic Acids Res.* **45**, 7326–7338 (2017).
26. Park, M. H., Cooper, H. L. & Folk, J. E. Identification of hypusine, an unusual amino acid, in a protein from human lymphocytes and of spermidine as its biosynthetic precursor. *Proc. Natl. Acad. Sci. USA* **78**, 2869–2873 (1981).
27. Abbruzzese, A., Park, M. H. & Folk, J. E. Deoxyhypusine hydroxylase from rat testis. Partial purification and characterization. *J. Biol. Chem.* **261**, 3085–3089 (1986).
28. Cano, V. S. et al. Mutational analyses of human eIF5A-1–identification of amino acid residues critical for eIF5A activity and hypusine modification. *FEBS J.* **275**, 44–58 (2008).
29. Nishimura, K., Lee, S. B., Park, J. H. & Park, M. H. Essential role of eIF5A-1 and deoxyhypusine synthase in mouse embryonic development. *Amino Acids* **42**, 703–710 (2012).
30. Wu, G. Q., Xu, Y. M. & Lau, A. T. Y. Recent insights into eukaryotic translation initiation factors 5A1 and 5A2 and their roles in human health and disease. *Cancer Cell Int.* **20**, 142 (2020).
31. Wang, Z., Jiang, J., Qin, T., Xiao, Y. & Han, L. EIF5A regulates proliferation and chemoresistance in pancreatic cancer through the sHH signalling pathway. *J. Cell Mol. Med.* **23**, 2678–2688 (2019).
32. Landau, G., Bercovich, Z., Park, M. H. & Kahana, C. The role of polyamines in supporting growth of mammalian cells is mediated through their requirement for translation initiation and elongation. *J. Biol. Chem.* **285**, 12474–12481 (2010).
33. Mathews, M. B. & Hershey, J. W. The translation factor eIF5A and human cancer. *Biochim. Biophys. Acta* **1849**, 836–844 (2015).
34. Liang, Y. et al. eIF5A hypusination, boosted by dietary spermidine, protects from premature brain aging and mitochondrial dysfunction. *Cell Rep.* **35**, 108941 (2021).
35. Puleston, D. J. et al. Polyamines and eIF5A hypusination modulate mitochondrial respiration and macrophage activation. *Cell Metab.* **30**, 352–363 (2019).
36. Schuller, A. P., Wu, C. C., Dever, T. E., Buskirk, A. R. & Green, R. eIF5A Functions globally in translation elongation and termination. *Mol. Cell* **66**, 194–205 (2017).
37. Matsumoto, K. et al. Chemical genetic interaction linking eIF5A hypusination and mitochondrial integrity. Preprint at https://doi.org/10.1101/2023.12.20.571781 (2023).
38. Ude, S. et al. Translation elongation factor EF-P alleviates ribosome stalling at polyproline stretches. *Science* **339**, 82–85 (2013).
39. Doerfel, L. K. et al. EF-P is essential for rapid synthesis of proteins containing consecutive proline residues. *Science* **339**, 85–88 (2013).
40. Doerfel, L. K. et al. Entropic contribution of elongation factor P to proline positioning at the catalytic Center of the ribosome. *J. Am. Chem. Soc.* **137**, 12997–13006 (2015).
41. Mudryi, V., Peske, F. & Rodnina, M. Translation factor accelerating peptide bond formation on the ribosome: EF-P and eIF5A as entropic catalysts and a potential drug targets. *BBA Adv.* **3**, 100074 (2023).
42. Huter, P. et al. Structural basis for polyproline-mediated ribosome stalling and rescue by the translation elongation factor EF-P. *Mol. Cell* **68**, 515–527 (2017).
43. Gray, N. K. & Hentze, M. W. Iron regulatory protein prevents binding of the 43S translation pre-initiation complex to ferritin and eALAS mRNAs. *EMBO J.* **13**, 3882–3891 (1994).
44. Melnikov, S. et al. Crystal structure of hypusine-containing translation factor eIF5A bound to a rotated eukaryotic ribosome. *J. Mol. Biol.* **428**, 3570–3576 (2016).
45. Lee, J. W., Bae, S. H., Jeong, J. W., Kim, S. H. & Kim, K. W. Hypoxia-inducible factor (HIF-1)alpha: its protein stability and biological functions. *Exp. Mol. Med.* **36**, 1–12 (2004).
46. Juszkiewicz, S. et al. ZNF598 Is a quality control sensor of collided ribosomes. *Mol. Cell* **72**, 469–481.e467 (2018).
47. Kim, J. H. et al. High cleavage efficiency of a 2A peptide derived from porcine teschovirus-1 in human cell lines, zebrafish and mice. *PLoS ONE* **6**, e18556 (2011).
48. Koutmou, K. S. et al. Ribosomes slide on lysine-encoding homopolymeric A stretches. *Elife* **4**, https://doi.org/10.7554/elife.05534 (2015).
49. Machida, K. et al. A translation system reconstituted with human factors proves that processing of encephalomyocarditis virus proteins 2A and 2B occurs in the elongation phase of translation without eukaryotic release factors. *J. Biol. Chem.* **289**, 31960–31971 (2014).
50. Machida, K. et al. Dynamic interaction of poly(A)-binding protein with the ribosome. *Sci. Rep.* **8**, 17435 (2018).
51. Yokoyama, T. et al. HCV IRES Captures an actively translating 80S ribosome. *Mol. Cell* **74**, 1205–1214.e1208 (2019).
52. Tesina, P. et al. Molecular basis of eIF5A-dependent CAT tailing in eukaryotic ribosome-associated quality control. *Mol. Cell* **83**, 607–621 (2023).
53. Hashimoto, S., Sugiyama, T., Yamazaki, R., Nobuta, R. & Inada, T. Identification of a novel trigger complex that facilitates ribosome-associated quality control in mammalian cells. *Sci. Rep.* **10**, 3422 (2020).
54. Kostova, K. K. et al. CAT-tailing as a fail-safe mechanism for efficient degradation of stalled nascent polypeptides. *Science* **357**, 414–417 (2017).
55. Tesina, P. et al. Molecular mechanism of translational stalling by inhibitory codon combinations and poly(A) tracts. *EMBO J.* **39**, e103365 (2020).
56. Chandrasekaran, V. et al. Mechanism of ribosome stalling during translation of a poly(A) tail. *Nat. Struct. Mol. Biol.* **26**, 1132–1140 (2019).
57. Schneider-Poetsch, T. et al. Inhibition of eukaryotic translation elongation by cycloheximide and lactimidomycin. *Nat. Chem. Biol.* **6**, 209–217 (2010).
58. Miyamoto, Y. et al. Identification of Saccharomyces cerevisiae isoleucyl-tRNA synthetase as a target of the G1-specific inhibitor Reveromycin A. *J. Biol. Chem.* **277**, 28810–28814 (2002).
59. Schmidt, C. et al. Structure of the hypusinylated eukaryotic translation factor eIF-5A bound to the ribosome. *Nucleic Acids Res.* **44**, 1944–1951 (2016).

60. Buschauer, R. et al. The Ccr4-Not complex monitors the translating ribosome for codon optimality. *Science* **368**, https://doi.org/10.1126/science.aay6912 (2020).
61. Mangano, K. et al. Context-based sensing of orthosomycin antibiotics by the translating ribosome. *Nat. Chem. Biol.* **18**, 1277–1286 (2022).
62. Li, W. et al. Structural basis for selective stalling of human ribosome nascent chain complexes by a drug-like molecule. *Nat. Struct. Mol. Biol.* **26**, 501–509 (2019).
63. Leroy, E. C., Perry, T. N., Renault, T. T. & Innis, C. A. Tetracenomycin X sequesters peptidyl-tRNA during translation of QK motifs. *Nat. Chem. Biol.* **19**, 1091–1096 (2023).
64. Zhang, Y. et al. The context of the ribosome binding site in mRNAs defines specificity of action of kasugamycin, an inhibitor of translation initiation. *Proc. Natl. Acad. Sci. USA* **119**, https://doi.org/10.1073/pnas.2118553119 (2022).
65. Svetlov, M. S. et al. Context-specific action of macrolide antibiotics on the eukaryotic ribosome. *Nat. Commun.* **12**, 2803 (2021).
66. Schroeder, S. et al. Dietary spermidine improves cognitive function. *Cell Rep.* **35**, 108985 (2021).
67. Stein, K. C., Morales-Polanco, F., van der Lienden, J., Rainbolt, T. K. & Frydman, J. Ageing exacerbates ribosome pausing to disrupt cotranslational proteostasis. *Nature* **601**, 637–642 (2022).
68. Singh, R., Sharma, M., Joshi, P. & Rawat, D. S. Clinical status of anticancer agents derived from marine sources. *Anticancer Agents Med. Chem.* **8**, 603–617 (2008).
69. Pavlovic Djuranovic, S. et al. Plasmodium falciparum translational machinery condones polyadenosine repeats. *Elife* **9**, https://doi.org/10.7554/elife.57799 (2020).
70. Juszkiewicz, S. & Hegde, R. S. Initiation of quality control during Poly(A) translation requires site-specific ribosome ubiquitination. *Mol. Cell* **65**, 743–750 (2017).
71. Dang, Y. et al. Inhibition of eukaryotic translation elongation by the antitumor natural product Mycalamide B. *RNA* **17**, 1578–1588 (2011).
72. Chhipi-Shrestha, J. K. et al. Splicing modulators elicit global translational repression by condensate-prone proteins translated from introns. *Cell Chem. Biol.* **29**, 259–275 (2022).
73. Mito, M., Mishima, Y. & Iwasaki, S. Protocol for disome profiling to survey ribosome collision in humans and zebrafish. *STAR Protoc.* **1**, 100168 (2020).
74. Shichino, Y. et al. eIF4A1 enhances LARP1-mediated translational repression during mTORC1 inhibition. *Nat. Struct. Mol. Biol.* **31**, 1557–1566 (2024).
75. Ingolia, N. T., Brar, G. A., Rouskin, S., McGeachy, A. M. & Weissman, J. S. The ribosome profiling strategy for monitoring translation in vivo by deep sequencing of ribosome-protected mRNA fragments. *Nat. Protoc.* **7**, 1534–1550 (2012).
76. Iwasaki, S., Floor, S. N. & Ingolia, N. T. Rocaglates convert DEAD-box protein eIF4A into a sequence-selective translational repressor. *Nature* **534**, 558–561 (2016).
77. Wu, X. & Bartel, D. P. kpLogo: positional k-mer analysis reveals hidden specificity in biological sequences. *Nucleic Acids Res.* **45**, W534–W538 (2017).

Acknowledgements

We thank members of the Yoshida and Iwasaki labs for constructive discussions and technical help, especially Mari Mito for providing helpful technical advice on ribosome profiling, as well as Hironori Saito and Peixun Han for help with data processing. Ken Matsumoto and Rumi Kurokawa provided helpful insights and constructive comments on experimental data. We are indebted to Kenji Ohtawa of the RIKEN Center for Brain Science for FACS analysis.

T.S.P. was supported by a RIKEN Shorei Incentive Research Projects Grant.

M.Y. was supported in part by a Grant-in-Aid for Scientific Research (S) (JP19H05640) and (JP23H05473) from the Japan Society for the Promotion of Science (JSPS) and Grant-in-Aid for Scientific Research on Innovative Areas (JP18H05503) and a Grant-in-Aid for Transformative Research Areas (A) "Chronoproteinology", (JP23H04882) from the Ministry of Education, Culture, Sports, Science and Technology (MEXT). S.I. was supported by the Japan Agency for Medical Research and Development (AMED) (AMED-CREST, JP20gm1410001), (JSPS) [a Grant-in-Aid for Scientific Research (B), JP23H02415], (MEXT) [a Grant-in-Aid for Transformative Research Areas (B) "Parametric Translation", JP20H05784; a Grant-in-Aid for Transformative Research Areas (A), JP24H02307] and RIKEN (Pioneering Projects "Biology of Intracellular Environments"). Y.S. was supported by JSPS [a Grant-in-Aid for Scientific Research (C), JP23K05648], MEXT [a Grant-in-Aid for Transformative Research Areas (A) "Multifaceted Proteins", JP21H05734, JP23H04268] and RIKEN (Pioneering Projects "Biology of Intracellular Environments"). T.I. was supported by AMED [AMED-CREST, JP23gm1410001 (to S.I. and T.I.)], MEXT [a Grant-in-Aid for Transformative Research Areas (A), JP21H05281], and RIKEN (Pioneering Projects "Biology of Intracellular Environments"). Support from NIH NIGMS (R35 GM134910) to D.R. is gratefully acknowledged.

Author contributions

Conceptualization and Methodology, T.S.P and Y.D.; Software, S.I., Y.S., and T.S.P.; Investigation, T.S.P, Y.D., W.I., and M.A. Resources, S.I., A.A.M., C.M., and D.R.; Writing – Original Draft, T.S.P; Review and Editing, T.S.P., S.I., Y.D., Y.S., and M.Y. Project Administration and Supervision, T.S.P., M.Y., J.O.L, S.I., and T.I.; Funding Acquisition, M.Y., S.I., T.I., Y.S., and T.S.P.

Competing interests

The authors declare no competing interests.

Additional information

Supplementary information The online version contains supplementary material available at https://doi.org/10.1038/s41467-024-54838-2.

Correspondence and requests for materials should be addressed to Tilman Schneider-Poetsch or Minoru Yoshida.

Peer review information *Nature Communications* thanks the anonymous reviewers for their contribution to the peer review of this work. A peer review file is available.